JOURNAL OF AEROSPACE COMPUTING, INFORMATION, AND COMMUNICATION
Vol. 6, September 2009

Allocation of Radar Tracking Resources by Direct Optimization

Joseph Z. Ben-Asher*
Technion—Israel Institute of Technology, Haifa 32000, Israel
and
Dror Cohen
Wales, Ltd., Ramat-Gan 52522, Israel
DOI: 10.2514/1.36567

The problem of optimal allocation of radar resources is addressed. Open-loop optimal strategies are obtained by direct optimization. The satisfaction of the Maximum Principle is verified by a noniterative process. The structure of the solutions is investigated by extensive numerical solutions and the main features of the optimal strategies are characterized.

I. Introduction

A ballistic missile defense (BMD) system uses its sensors for various missions such as detection and acquisition, tracking, fire control, etc.

Missions "compete" over the same finite stockpile of sensor resources and have to be performed within certain time intervals. Mission performance level depends on the amount of sensor resources allocated to it, and therefore can be optimized by specific allocation. In general, optimality criteria of sensor resource allocation may be scenario dependent.

An interim problem of the general resource optimization problem is radar tracking beam allocation. Classically, the objective of the sensor allocation process in tracking has been to minimize the uncertainty in the tracking estimation error of all relevant targets, using a given amount of radar resources. The first efforts to solve this problem took place in the sixties and early seventies of the last century. Athans and Schweppe [1] used the Kalman–Bucy theory to formulate an optimization problem for a single target where the states of the problem are the elements of the target's covariance matrix. The problem was constrained by the total amount of energy used and by the maximal peak power. The Maximum Principle was employed to derive the optimal on–off solution to the problem. A simpler model had been used by Schweppe and Gray [2], where the special case of a one-dimensional problem was considered under some simplifying assumptions. Some basic structures of the optimal allocation have been revealed for constant velocity and constant acceleration targets.

The next profound effort was the work of Heffes and Horing [3]. They considered the general case of multiple targets with different trajectories, and proposed an iterative algorithm to solve the two-point boundary-value problem (TPBVP) derived from the Maximum Principle. The allocation of each and every pulse in open loop is done in a repeatable fashion. In realistic BMD scenarios to solve the TPBVP for every pulse is a formidable effort and it seems that for this reason this line of research has been abandoned. Instead, dynamic programming approaches have been employed to the problem. The shortcoming of these closed-loop methods is that the structure of the solution can no longer be easily observed and heuristically understood.

Received 10 January 2008; accepted for publication 4 June 2009.
* Department of Aerospace Engineering, Technion—Israel Institute of Technology, Haifa 32000, Israel, yossi@aerodyne.technion.ac.il.

In recent years, there have been many works on using direct optimization tools to solve optimal control problems [4–6]. The solutions are obtained by nonlinear programming (NLP) solvers and are verified by the Maximum Principle. Our present work employs Heffes and Horing's modeling assumptions and problem formulation and adds two main contributions: a) the problem is solved by a direct optimization approach (unlike the indirect approach of [3]) with the Maximum Principle serving as a a-posteriori verification tool; and b) the structure of the solution is thoroughly investigated and the main features of the solution are identified.

The paper is organized as follows. Section II formulates the problem and the necessary conditions for optimality. Section III proposes the direct optimization approach. In Sec. IV and Sec. V results are given for a single target and multiple targets, respectively, and the main features are explored. Section VI concludes the paper.

II. Problem Formulation and Analysis

We search for the optimal allocation of radar pulses to targets being tracked. The objective function for the optimization is a function of the estimation error covariance matrix.

The following equation is a basic model for the evolution of the state estimation error covariance matrix [4]

$$X_j(i+1) = f_j(X_j(i), \quad u_j(i)), \quad i = 1, \ldots, N-1, \ j = 1, \ldots, n \tag{1}$$

where $u_j(i)$ is a binary number indicating which target is pulsed at time step i; X_j is the predicated error covariance matrix of target j at a certain (fixed) future (discrete) time N'; and N is the number of tracking time steps (thus $N \leqslant N'$). There are n ballistic targets, not necessarily identical.

Using a linearized Kalman filter (KF) [7], where the linearization is around a nominal ballistic trajectory, the set of equations for radar tracking a ballistic target can be further written as follows [3]

$$X_j(i+1) = X_j(i) - u_j(i)G_j(X_j(i), i) \quad i = 1, \ldots, N, \ j = 1, \ldots, n \tag{2}$$

Here again, the control variables $u_j(i)$ are binary variables that indicate whether the radar directs energy at (i.e., "pulses") the jth target at time t_i; G_j represents the improvement in the prediction accuracy which would result from the assignment of the radar at the ith step to the jth target. For the complete modeling and a derivation of G_j, see Appendix A.

For simplicity, we assume that the radar dwell time and the KF time step are identical. Thus only one target can be pulsed during the KF time interval $[t_i, t_{i+1}]$.

The objective is to minimize a weighted sum of certain functions of the targets' estimation error covariance matrix; thus the optimization objective function can be written as follows

$$J = \sum_{j=1}^{n} w_j f_0(X_j(N')) \tag{3}$$

where f_0 is a function of the information state at $N' \geqslant N$, and w_j is a weighting factor for the jth target.

Remark: For operational reasons, we might be more interested in the equivalent problem of minimizing the total radar resources subject to a given (prescribed) accuracy. Appendix B addresses this formulation.

A discrete time Maximum Principle can be employed, provided the control set is convexified. Since the control appears linearly in the state equation, the solution will nevertheless belong to the admissible set of unit vectors. (Note that in case of a global constraint on the radar resources we assume that it is expressed as an integer number

of allocation steps.) The following TPBVP results [8]

$$
\begin{aligned}
H(X,\lambda,\eta) &= \sum_{j=1}^{n} -\mathrm{tr}[\eta_j(i)G_j(X_j(i),i)\lambda_j^{\mathrm{T}}(i+1)] + \lambda_0 \sum_{j=1}^{n}\sum_{i=1}^{N'} \eta_j(i) \\
\lambda_j(i+1) - \lambda_j(i) &= -\left[\frac{\partial H}{\partial X}\right]_j \\
\lambda_j(N) &= w_j \frac{\partial f_0}{\partial X_j} \\
u(i) &= \underset{0\leqslant\eta(i)\leqslant 1}{\arg\min}\, H(X,\lambda,\eta)
\end{aligned}
\tag{4}
$$

where $\frac{\partial H}{\partial X}$ is the so called "gradient matrix" whose (k,l) element is given by $\frac{\partial H}{\partial x_{kl}}$,where x_{kl} is the (k,l)th element of X. Note that $\lambda_0 \neq 0$ if there is a global constraint and zero otherwise.

III. Direct Optimization Approach

In order to study the nature of the optimal strategies by direct optimization, and to keep the dimension of the problem small, we will search for approximate solutions.

To this end, we subdivide the tracking period into a relatively small number of segments L, each segment comprises an equal number of KF steps. Under this approximation, the control policy over each time segment $[t_l, t_{l+1}]$, $l = 0, \ldots, L-1$, is fixed (piecewise constant control). A new control variable $p_{l,j}$, indicates the *fraction* of the radar occupation time allocated to the jth target during the time interval $[t_l, t_{l+1}]$. In fact, $p_{l,j}$ represents all combinations of a fix number of pulses allocated the target j over that interval.

Further, we will use the following *approximation* to Eq. (2)

$$
\begin{aligned}
X_j(i+1) &= X_j(i) - p_j(i)G_j(X_j(i),i) \\
p_j(i) &= p_{j,l} \quad \text{for } i\cdot \mathrm{d}t \in [t_l, t_{l+1}],\ l = 0,1,\ldots,L-1
\end{aligned}
\tag{5}
$$

where $\mathrm{d}t$ is the time step of the KF (and, by assumption, also the radar dwell time).

Note again that the exact modeling for the covariance propagation (2) should use

$$
u_j(i) = \begin{cases} 1 & \text{if target } j \text{ is pulsed} \\ 0 & \text{otherwise} \end{cases}
$$

for each KF step. Here we propose using a fixed value $0 \leqslant p_j(i) \leqslant 1$ in the covariance propagation equation over the entire time interval $[t_l, t_{l+1}]$.

Before we go on, we should justify the need for approximation. Suppose that we have a tracking period of 50 s with the KF propagating in steps equal to the radar dwell time of, say, 100 ms. We then have a total sum of 500 pulses for allocation to all targets. Even if we know the number of pulses needed per target (which we do not), say it is 20, we still have

$$
\binom{500}{20} = 5.6 \times 10^{20}
$$

combinations to check for!

On the other hand, by subdividing the tracking period into 10 segments of 5 s each, we get only $10n$ unknowns (10 for each target) to deal with and optimize. Even with dozens of targets, it is a tractable NLP problem that can be solved in real time.

To validate the approximation, we will compare three simulation runs of a single target with KF steps of $\mathrm{d}t = 0.1$ s:

1) Solving Eq. (2) with u alternating each step (10 Hz) between 0 and 1.

2) Solving Eq. (2) with u alternating in 1 Hz between 0 and 1.
3) Solving Eq. (5) with $p = 0.5$.

In 1) we assume that during a 0.1 s interval the radar is pulsing the target, while the following 0.1 s interval the radar is not pulsing the target, and the next 0.1 s interval the radar is pulsing the target again, etc. We assume that the target's state estimate is updated for intervals in which the radar is pulsing the target, and simply propagated forward in time, using the dynamics of the target motion, when the radar does not pulse the target. For clarification, the radar pulsing needs the full 0.1 s and then we only get one measurement update for the KF.

In 2) we assume that during a 1.0 s interval the radar is pulsing the target, while the following 1 s interval the radar is not pulsing the target, etc. The radar dwell time remains 0.1 s, thus we get 10 consecutive KF updates, followed by 10 steps of propagation without measurements using the dynamics of the target motion.

In 3) we propagate the KF using Eq. (5). Recall that this is never the case with the actual KF, since Eq. (5) introduces one-half of the update due to measurement in each step. (One way to think of it, is as if the radar dwell time is now 0.05 s in stead of 0.1 s. Note that a more exact way to consider shorter dwells would be to change the radar covariance measurement matrix R, but then we lose the simple control-affine formulation of (5) which enables solving the problem *and* proving optimality conditions.

Finally, the following two facts should be noticed: a) this is only an approximation, as the actual improvement of the radar accuracy with dwell time cannot be described in such a simple way; and b) the optimal solution yields mostly $p_{j,l} = 1$ or 0 and interior values with $0 < p_{j,l} < 1$ appear in just a few time segments.

The results in terms of the predicted radial error uncertainty ($1\sigma_r$) at the end of a tracking period ($t = 20$ s) are within 5% accuracy (see Fig. 1).

Note that we present the predicted radial error uncertainty, hence when no measurements are taken, it remains constant. The current radial error uncertainty is increasing during these intervals but not the predicted one since this increase is already taken into account in the prediction. For example, at $t = 11$ s observe that the predicted uncertainty by method 2) remains about 300 m. At the beginning of this step we predict from current uncertainty to 9 s ahead ($t = 20$ s), thus propagating 90 steps using Eq. (A4)

$$\begin{aligned} P &= M \\ M &= APA^{\mathrm{T}} + LQL^{\mathrm{T}} \end{aligned} \tag{6}$$

At $t = 12$ s the current uncertainty has increased by 10 steps of no measurement. However, we have only 8 s (thus only 80 steps) to go till the prediction time. Clearly, the predicted covariance remains constant during this time interval.

We therefore formulate the following NLP problem

Find the set $\tilde{p} = \{p_{j,l} \geqslant 0;\ j = 1, \ldots, n,\ l = 0, \ldots, L-1\}$ such that

$$\min_{\tilde{p}} J$$

subject to L local constraints

$$P_l \equiv \sum_{j=1}^{n} p_{j,l} \leqslant 1, \quad l = 0, \ldots, L-1$$

and to the global constraint

$$\sum_{l=0}^{L-1} P_l \geqslant P_T$$

After solving this NLP problem we should also verify the optimality of the solution by checking for condition (4). The Lagrange's multipliers and a control switching function can be directly obtained from the solution (no iterations

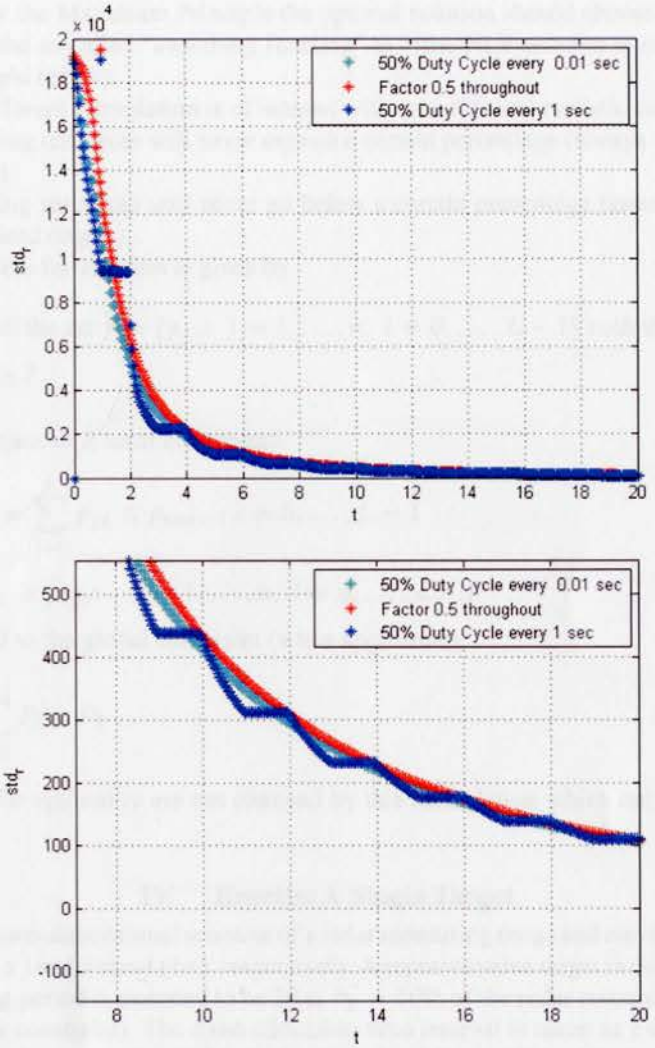

Fig. 1 Validating the approximation.

are needed) by the following recursion (see [3] and Appendix A)

$$\begin{aligned}
\lambda_j(i) &= \lambda_j(i+1) + \frac{\partial H}{\partial X_j} = (I - u_j(i)S_j(i))\lambda_j(i+1)(I - u_j(i)S_j(i))^{\mathrm{T}} \\
G_j(i) &= X_j(i)S_j(i) \\
m_j &\equiv \mathrm{tr}(G_j(x_j(i), i)\lambda_j^{\mathrm{T}}(i+1)) \\
u(i) &= \underset{0\leqslant\eta(i)\leqslant 1}{\arg\min}\, H(X, \lambda, \eta)
\end{aligned} \tag{7}$$

where (under our approximation) the control is piecewise constant, thus we have

$$u_j(i) = p_{j,l} \quad \forall i \cdot \mathrm{d}t \in [t_l, t_{l+1}]$$

Note that in order to satisfy the Maximum Principle the optimal solution should choose the target and the timings with the highest values of the so-called "switching function" m_j (the NLP solution is therefore checked to satisfy this requirement; see example below).

In practice, a slightly different formulation is of interest with two different realistic constraints:

1) The maximal tracking resources will never exceed a certain percentage (always leaving room for detection and other missions).
2) The minimal tracking resources will never go below a certain percentage (assuring a minimal pulsed and avoid losing un-pulsed targets).

Therefore the revised problem formulation is given by

Find the set $\tilde{p} = \{p_{j,l};\ j = 1, \ldots, n,\ l = 0, \ldots, L-1\}$ such that

$$\min_{\tilde{p}} J$$

subject to L local constraints

$$P_l \equiv \sum_{j=1}^{n} p_{j,l} \leqslant p_{\max}, \quad l = 0, \ldots, L-1$$

$$p_{j,l} \geqslant p_{\min}; \quad j = 1, \ldots, n,\ l = 0, \ldots, L-1$$

and to the global constraint (when applicable)

$$\sum_{l=0}^{L-1} P_l \geqslant P_T$$

The necessary conditions for optimality are not changed by this formulation which only affects the bounds of the control set.

IV. Results: A Single Target

Assume for simplicity a two-dimensional scenario of a radar measuring range and elevation with a fixed zero mean Gaussian noise of 100 m (1σ) and 1 mrad (1σ), respectively. A representative target is detected at a range of 800 km from the radar. The tracking period is assumed to be 20 s; $P_T = 50\%$ of the radar resources are allocated to tracking the target (global resources constraint). The fixed-allocation time interval is taken as 1 s. We want to minimize the (radial) position error uncertainty at a certain future time T_p s (in this case $T_p = N' \cdot \mathrm{d}t$). We will deal first with the simpler original formulation with $0 \leqslant p_{j,l} \leqslant 1$.

Time histories of the prediction error uncertainty for $T_p = \{20, 50, 100\}$ s are shown in Figs. 2–4, where the piecewise constant p presented on the same plots, with a scale as depicted by the arrows. The optimal results at the end of tracking ($1\sigma_r$) are {79, 280, 656} m, respectively (piecewise constant lines indicate the allocation decision and the continuous curves indicate the concomitant prediction error uncertainty).

The following phenomena can be observed:

1) When the prediction time (T_p) is at 20 s, most resources are near the end; the rest is at the beginning. The solution is of a 1–0 type (on–off). Note that the prediction error uncertainty does not vary during the "0" period.
2) When the prediction time is at 50 s, more resources are near the beginning. Note that partial allocation ($p < 1$) is now optimal.
3) When the prediction time is at 100 s, resources are equally shared between the beginning and the end of the tracking period. This result *is not changed* with further increasing of the prediction time, hence we may call it the "asymptotic allocation".

To understand the nature of the asymptotic allocation we study the problem of minimizing the *velocity* error uncertainty at $t = 20$ s (the end of the tracking period). The allocation results are given in Fig. 5, with the final error uncertainty ($1\sigma_v$) of 2.7 m/s.

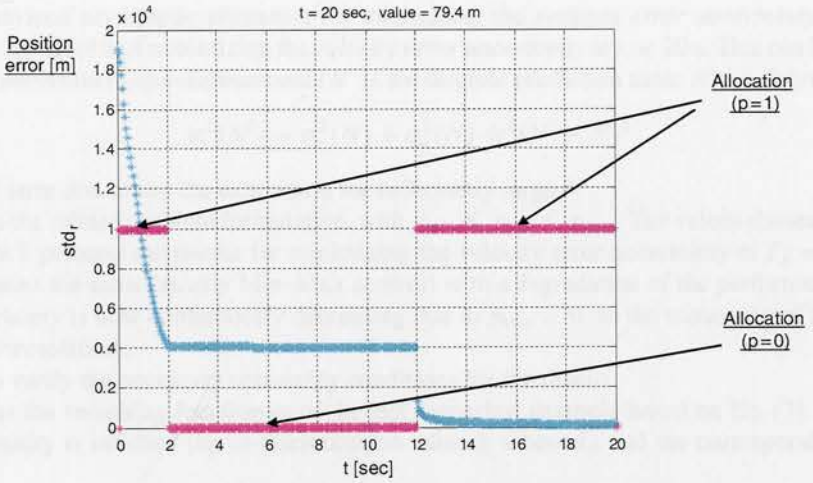

Fig. 2 Position error uncertainty at $T_p = 20$ s.

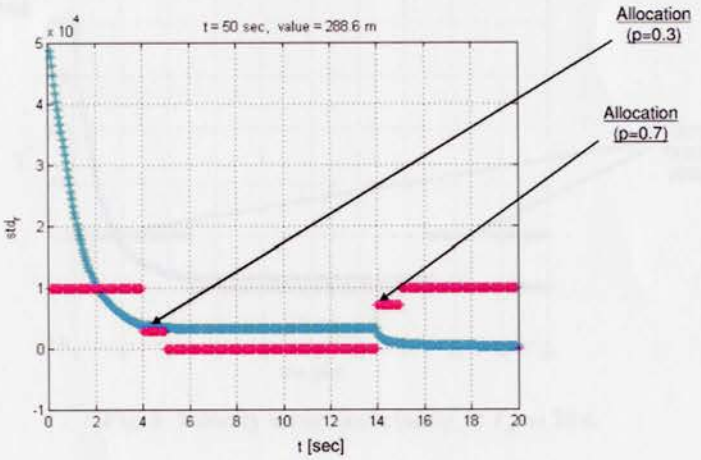

Fig. 3 Position error uncertainty at $T_p = 50$ s.

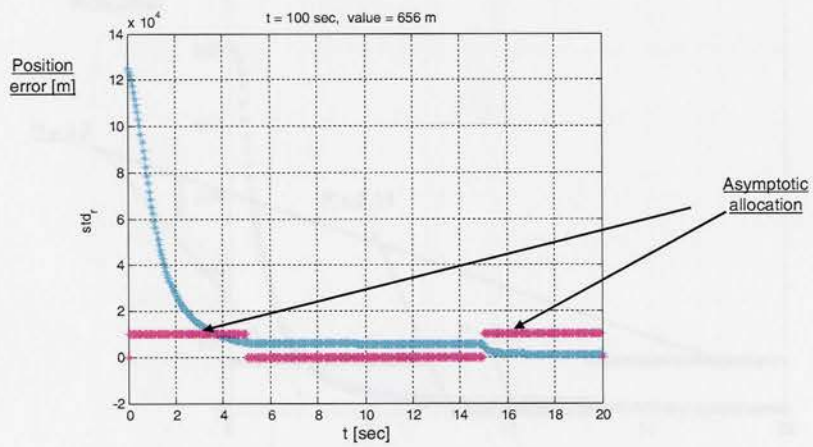

Fig. 4 Position error uncertainty at $T_p = 100$ s.

Note that the previous asymptotic allocation for minimizing the *position error uncertainty* at large prediction times is obtained as the results of minimizing the *velocity error uncertainty* at $t = 20$ s. This can be readily explained by the following observation in one-dimensional (N' is the discrete prediction time; N the discrete tracking period)

$$\sigma_r^2(N') = \sigma_r^2(N) + \sigma_v^2(N)\, \mathrm{d}t^2(N' - N)^2 \tag{8}$$

Clearly, the second term dominates the expression for sufficiently large N'.

We now turn into the refined problem formulation, with $p_{\min} \leqslant p_{j,l} \leqslant p_{\max}$. The values chosen are $p_{\max} = 0.7$ and $p_{\min} = 0.01$. Figure 6 presents the results for minimizing the velocity error uncertainty at $T_p = 20$ s. The structure of the solution remains the same (mostly Min–Max control) with a degradation of the performance by 13.5%. Note that the error uncertainty is now continuously decreasing due to $p_{\min} > 0$. In the remaining of this section, we will retain this revised formulation.

Next we need to verify the necessary optimality conditions for the results.

Figure 7 presents the switching function m of the last numerical example based on Eq. (7). It is shown that the condition for optimality is satisfied (up to discretization values), where λ_0 and the corresponding threshold for m

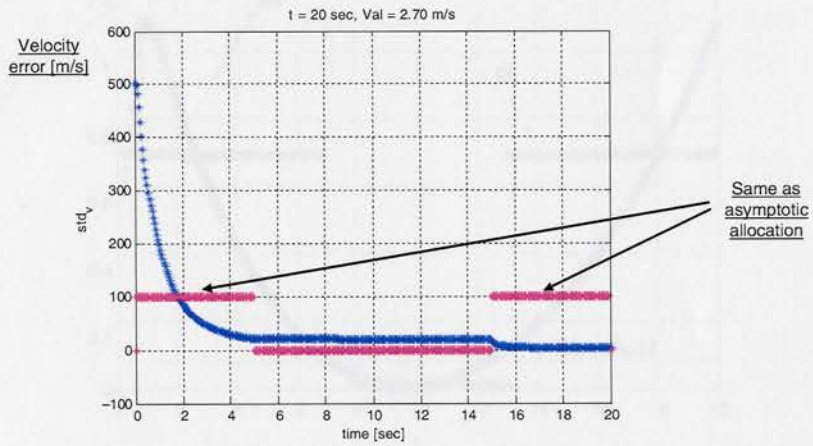

Fig. 5 Velocity error uncertainty at $T_p = 20$ s.

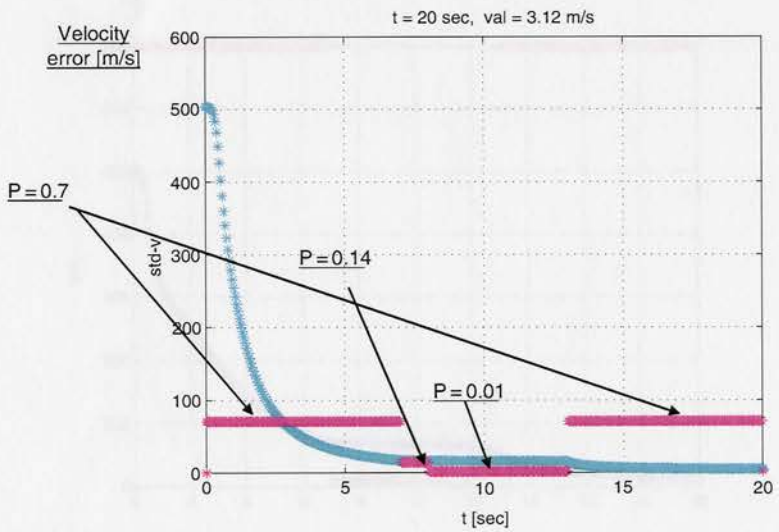

Fig. 6 Velocity error uncertainty at $T_p = 20$ s; single target; new local constraints.

are determined by the global constraint ($P_T = 50\%$). Note that the values $p_{\max} = 0.7$, $p_{\min} = 0.01$ do not allow for a pure Max–Min allocation, thus at least one segment requires partial allocation. The switching function m should cross the threshold during this segment.

Next we want to further investigate the structure of the optimal allocation. We start by increasing the angular measurement noise. The above results used 1 mrad for this value. Figures 8–10 present the results for 5, 10, and 20 mrad, respectively.

We have obtained two structures essentially Max–Min–Max for the lower angular measurements noise level, and essentially Max–Min–Max–Min–Max for the higher levels. Figure 11 presents the switching function for the last case to verify its optimality.

In the above examples we have kept constant the range measurement error and only changed the angular one. Decreasing the range standard deviation error from 100 to 5 m (maintaining the nominal elevation error of 1 mrad)

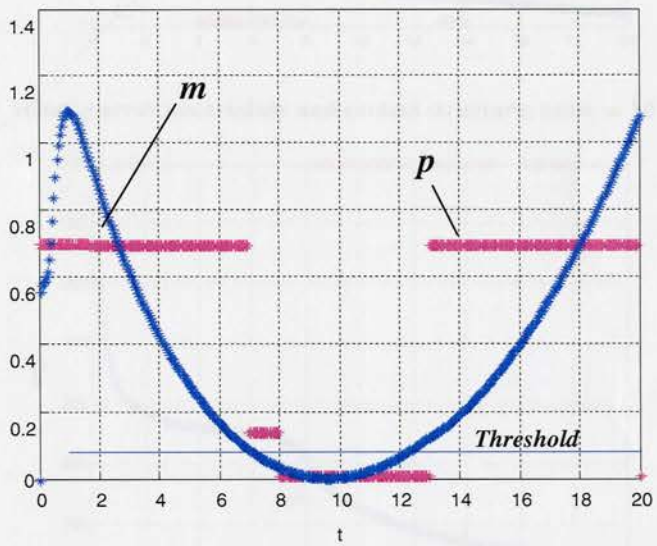

Fig. 7 Switching function (nominal case).

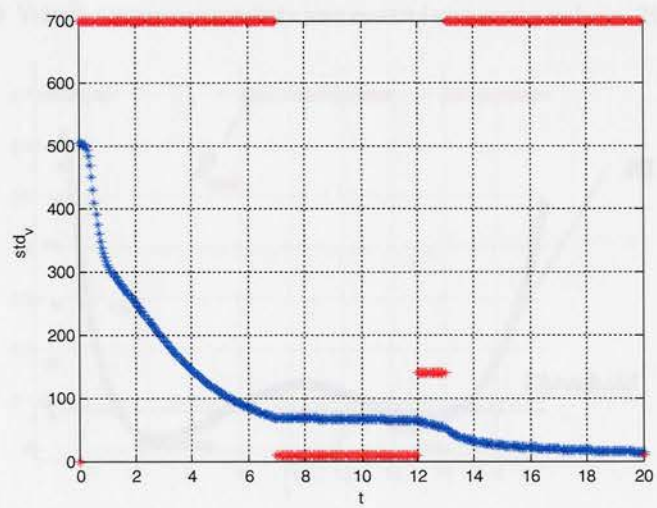

Fig. 8 Velocity error uncertainty and control structure; noise = 5 mrad.

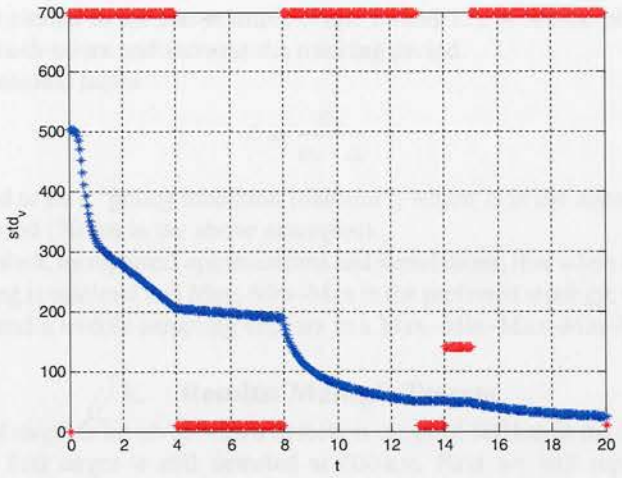

Fig. 9 Velocity error uncertainty and control structure; noise = 10 mrad.

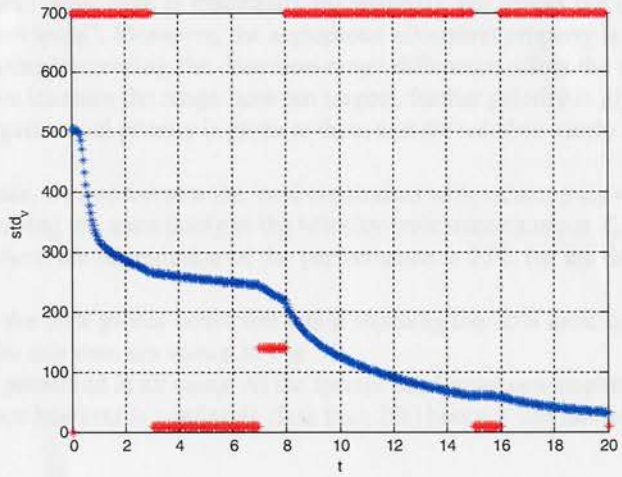

Fig. 10 Velocity error uncertainty and control structure; noise = 20 mrad.

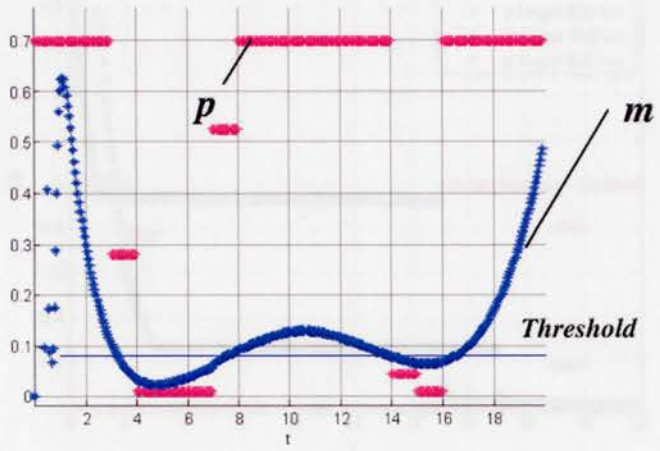

Fig. 11 Switching function (high angular noise).

yields an allocation structure similar to the last example (Figs. 10 and 11). A similar phenomenon occurs when we keep the nominal values for both errors and increase the tracking period.

Consequently, a nondimensional factor

$$\delta \equiv \frac{\sigma_r}{\sigma_\theta \cdot \Delta} \tag{9}$$

has been empirically revealed to be a "policy transition indicator", where Δ is the distance traveled by the target in the course of the tracking period (70 km in the above examples).

It was numerically established, by repeated optimizations and simulations, that when δ is close to 1—the improvement due to midpoint sampling is minimal and Max–Min–Max is the preferred strategy; whereas when δ gets smaller (say 0.1) the reverse is true, and a middle sampling appears in a Max–Min–Max–Min–Max structure.

V. Results: Multiple Targets

Assume now that a second target is involved with a detection range of 500 km at the (joint) time of the beginning of the tracking period. The first target is still detected at 800 km. First we will repeat the investigation of the predicted position uncertainty for various prediction times with no additional local constraints. The above three cases $T_p = \{20, 50, 100\}$ s are shown in Figs. 12–14, respectively. The allocation resembles the single target allocation (mostly on–off, where the joint dead zone is essentially maintained), but favors the distant target (less accurate) and provides it with the "sweet spots". Moreover, the asymptotic allocation property is essentially preserved as can be seen from Fig. 15. Increasing/decreasing the detection-range difference affect the results as shown in Figs. 16 and 17, respectively. When we increase the range between targets, further priority is given to the distant target. For the case of closely spaced targets, equal priority is given to them and the solution nearly equalizes the predicted error uncertainty (2.7–2.75 m/s).

As with the single target case, we impose now the local constraints with values: $p_{\max} = 0.7$, $p_{\min} = 0.01$. Figure 18 presents the results for minimizing the uncertainty in the velocity error uncertainty at $T_p = 20$ s. The structure of the solution remains the same where the degradation of the performance is 25% for the double target case (13.5% for the single target case).

It is interesting to remove the 50% *global* constraint while retaining the 70% local constraints (a trivial case with a single target). The results for this case are shown in Fig. 19.

The nature of the result is preserved in all cases. At the former dead-zone new nonbinary allocation is developed. Its contribution to performance however is negligible (less than 2%) hence it can be treated as "garbage time".

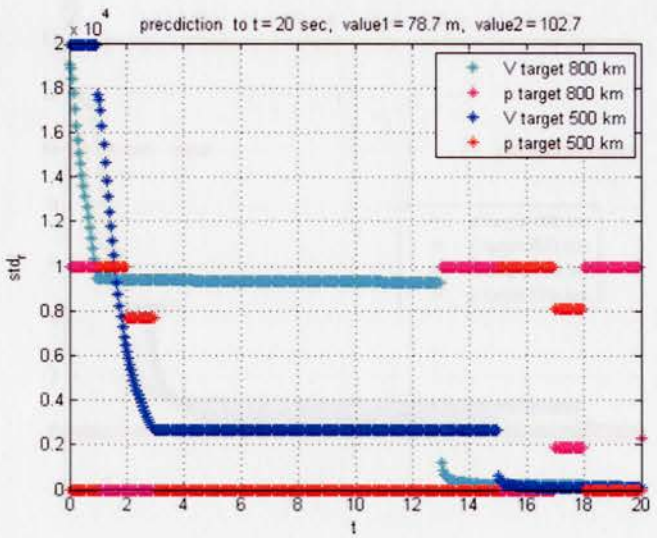

Fig. 12 Predicted position error uncertainty at $T_p = 20$ s.

Verifying optimality with multiple targets is more elaborate. We need to show that the optimal solution chooses the target and the timings with the highest values of the index function m_j in order to satisfy the Maximum Principle. Figure 20 presents the results for the optimal allocation and the corresponding m_j in the problem of minimizing the velocity error uncertainty at $t = 20$ s for two targets detected at 800 km with a different Radar Cross Section entailing a different measurement noise: for target 1, $\sigma_\theta = 0.005$ and for target 2, $\sigma_\theta = 0.001$. The Maximum Principle is satisfied during the Max–Min allocation zones. The (unavoidable) partial allocation zone at $t = 17$ s does not strictly comply with this condition: m_1 and m_2 are very close but still $m_1 > m_2$ and yet the allocation is reversed $p_1 < p_2$. A considerable effort to redeem this situation revealed that it is highly sensitive, and very small changes in the allocation strategies cause tremendous changes in m_i, violating the Maximum Principle throughout the solution. Hence the approximation scheme here seems to be is suboptimal.

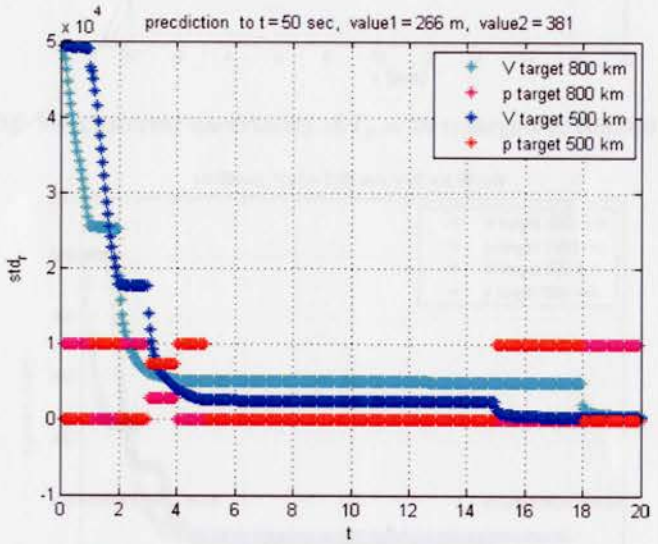

Fig. 13 Predicted position error uncertainty at $T_p = 50$ s.

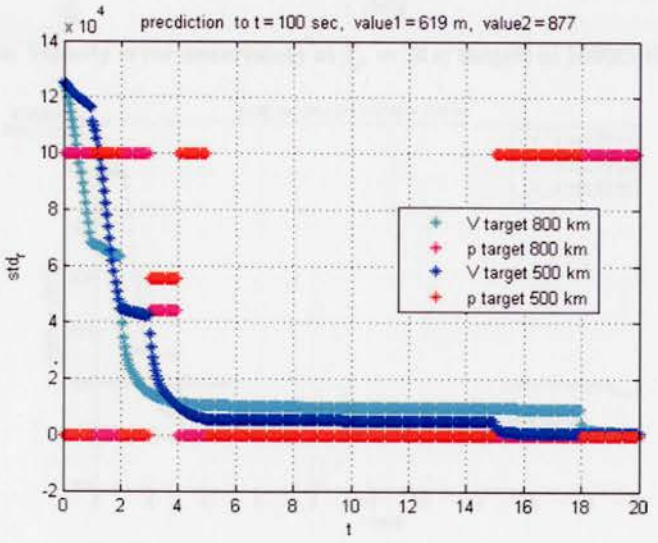

Fig. 14 Predicted position error uncertainty at $T_p = 100$ s.

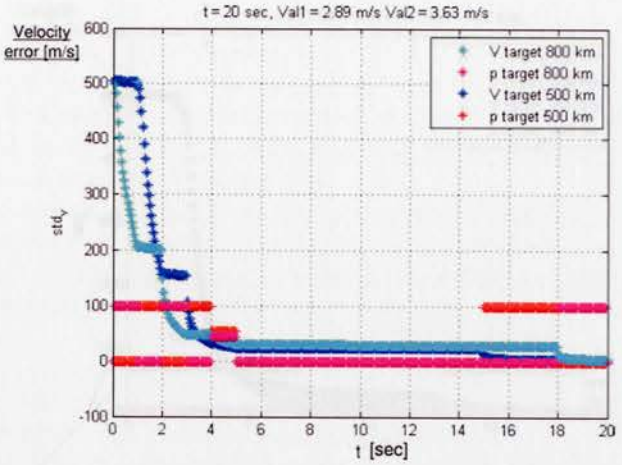

Fig. 15 Velocity error uncertainty at $T_p = 20$ s; targets at 800/500 km.

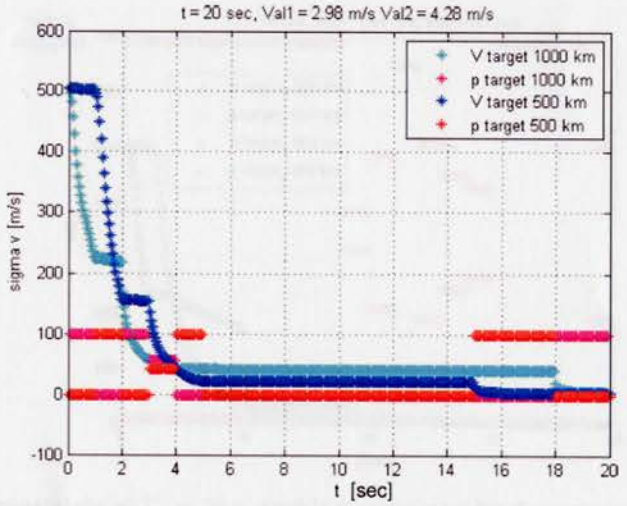

Fig. 16 Velocity error uncertainty at $T_p = 20$ s; targets at 1000/500 km.

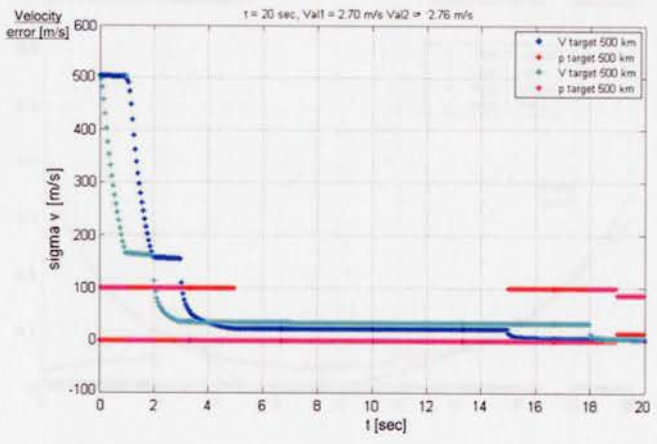

Fig. 17 Velocity error uncertainty at $T_p = 20$ s; both targets at 500 km.

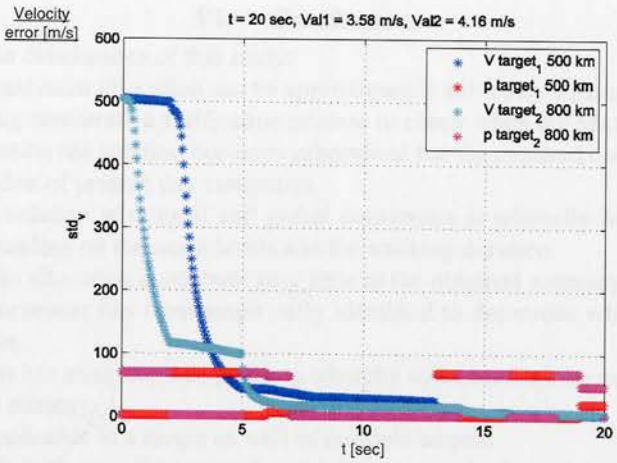

Fig. 18 Velocity error uncertainty at $T_p = 20$ s; double targets; new local constraints.

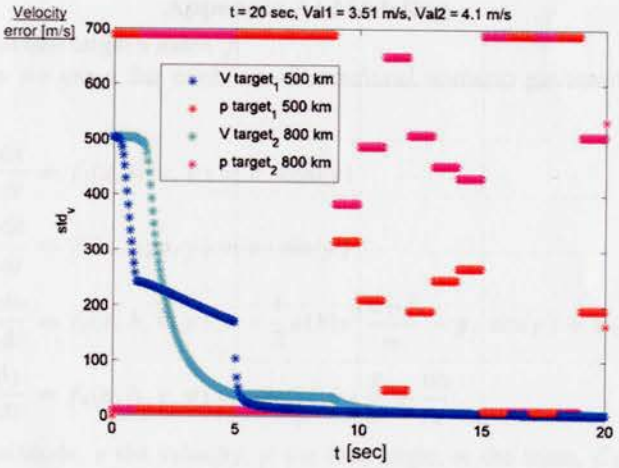

Fig. 19 Velocity error uncertainty at $T_p = 20$ s; double targets; new local constraints; no global constraint.

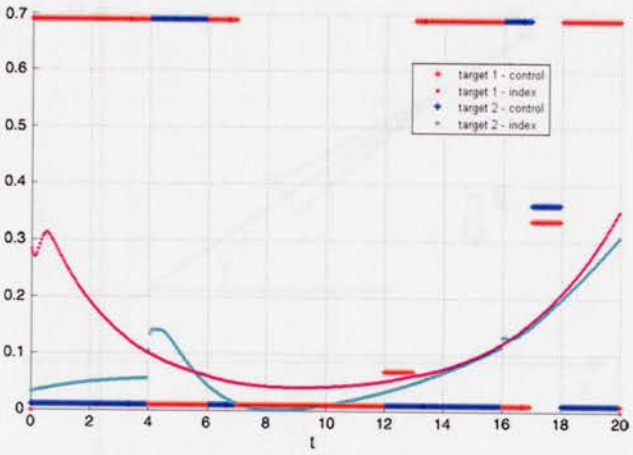

Fig. 20 Switching functions for two targets.

VI. Conclusions

The following are the main conclusions of this study:

1) The problem of optimal radar allocation can be approximately solved by a parameter optimization approach with an accompanying noniterative verification process to check when the Maximum Principle is satisfied.
2) Due to the approximation the solution becomes suboptimal but the required computational effort is suitable for real-time application of present day computers.
3) The structure of the solution with local and global constraints is primarily Max–Min–Max–Min–Max or Max–Min–Max, depending on the noise levels and the tracking duration.
4) Time zones of the Min allocation contribute very little to the obtained accuracy.
5) A nondimensional parameter has been empirically identified to determine which of the main strategies is valid in a specific case.
6) The allocation process has an asymptotic property whereby solutions for long enough periods are converging to a single allocation strategy.
7) All of the above is applicable to a single as well as multiple targets.

Although the paper has dealt with two-dimensional scenarios, its results have been tested in three-dimensional scenarios as well, with a radar location on and off the ballistic plane. All of the above findings have been validated.

Appendix A: Modeling

For simplicity we will omit that target's index j.

For the target's dynamics we use a flat earth two-dimensional scenario governed by the following dynamic equations (Fig. A1)

$$\begin{aligned}
\frac{dx}{dt} &= f_1(x,h,v,\gamma) = v\cdot\cos(\gamma)\\
\frac{dh}{dt} &= f_2(x,h,v,\gamma) = v\cdot\sin(\gamma)\\
\frac{dv}{dt} &= f_3(x,h,v,\gamma) = -\frac{1}{2}\rho(h)v^2\frac{C_D S}{m} - g\cdot\sin(\gamma) + w_1\\
\frac{d\gamma}{dt} &= f_4(x,h,v,\gamma) = -\cos(\gamma)\cdot\frac{g}{v} + \frac{w_2}{v}
\end{aligned} \tag{A1}$$

where x is the range, h the altitude, v the velocity, γ the dive angle, m the mass, C_D the drag coefficient, S the reference area, ρ the density, g the gravity and w_1, w_2 are the disturbances.

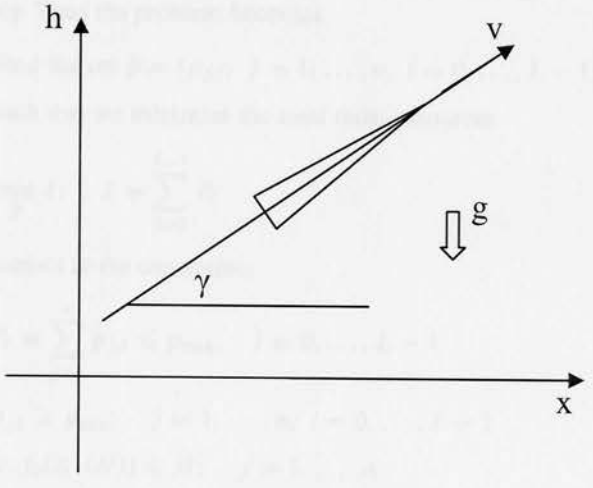

Fig. A1 States definition.

Let the radar measures slant rage and elevation angle to target. Thus we have

$$\begin{aligned} y_k &= \underline{g}_k + \underline{v}_k, \quad \underline{v}_k \sim N(0, R_k) \\ \underline{g}_k &= \begin{bmatrix} \Theta_k & r_k \end{bmatrix}^{\mathrm{T}} \\ \begin{bmatrix} \Theta_k \\ r_k \end{bmatrix} &= \begin{pmatrix} \arcsin\left(\frac{z_{r,k}-z_k}{r_k}\right) \\ \sqrt{(x_{r,k}-x_k)^2+(z_{r,k}-z_k)^2} \end{pmatrix} \end{aligned} \tag{A2}$$

where $()_k$ denotes values at discrete time k and $()_{r,k}$ denotes values of radar at this time; x, z are Cartesian coordinates ($z = -h$); Θ is the elevation; r the range.

To obtain the error uncertainty propagation equation, we linearize around a nominal trajectory and we get an expression for the covariance matrix P. When measurements are taken, we get the following improvement in the *current* covariance matrix:

$$\begin{aligned} P &= M - MC^{\mathrm{T}}[CMC^{\mathrm{T}} + R]^{-1}CM \\ M &= APA^{\mathrm{T}} + LQL^{\mathrm{T}} \\ A &= \frac{\partial f_i}{\partial x_j}; \quad C = \frac{\partial g_i}{\partial x_j} \\ L &= \begin{bmatrix} 0 & 0 & 1 & 0 \\ 0 & 0 & 0 & 1/v \end{bmatrix}^{\mathrm{T}}; \quad Q = \begin{bmatrix} \sigma_{w_1}^2 & 0 \\ 0 & \sigma_{w_2}^2 \end{bmatrix}; \quad R = \begin{bmatrix} \sigma_\theta^2 & 0 \\ 0 & \sigma_r^2 \end{bmatrix} \end{aligned} \tag{A3}$$

In the prediction step we use

$$\begin{aligned} P &= M \\ M &= APA^{\mathrm{T}} + LQL^{\mathrm{T}} \end{aligned} \tag{A4}$$

The value of G in Eq. (2) can be shown, after some calculations, to have the following form [3]

$$G(X(i), i) = X(i)[A^{N'-i}]^{-1}C^{\mathrm{T}}\left[C[A^{N'-i}]^{-1}X(i)[A^{N'-i}]^{-\mathrm{T}}C^{\mathrm{T}} + R\right]^{-1} C[A^{N'-i}]^{-1}X(i) \equiv X(i)S(i) \tag{A5}$$

Appendix B : Reversed Formulation

For operational reasons we might be interested in the problem of minimizing the integral radar resources subject to a given (prescribed) accuracy. Thus the problem becomes

Find the set $\tilde{p} = \{p_{j,l};\ j = 1, \ldots, n,\ l = 0, \ldots, L-1\}$

such that we minimize the *total* radar resources

$$\min_{\tilde{p}} J; \quad J = \sum_{l=0}^{L-1} P_l$$

subject to the constraints

$$P_l \equiv \sum_{j=1}^{n} p_{j,l} \leqslant p_{\max}, \quad l = 0, \ldots, L-1$$

$$p_{j,l} \geqslant p_{\min}; \quad j = 1, \ldots, n,\ l = 0, \ldots, L-1$$

$$w_j f_0(X_j(N)) \leqslant H; \quad j = 1, \ldots, n$$

The latter constraint is the weighted required accuracy.

The solutions turn out to be of the same structure. Moreover the problem of minimizing the predictive error uncertainty with imposed limited radar resources and the problem of minimizing the total radar resources for a given (required) accuracy are equivalent and a solution to one is also a solution to the other; this is a direct result of the monotonic dependency between the two values. In fact, each solution set {resources, accuracy} is a Pareto solution for the corresponding multiobjective optimization problem. We finally note that computation-wise there is no significant difference between the two problem formulations.

References

[1] Athans, M., and Schweppe, F. C., "On Optimal Waveform Design via Control Theoretic Concepts," *Information and Control,* Vol. 10, Oct. 1967, pp. 335–377.
doi: 10.1016/S0019-9958(67)90183-0

[2] Schweppe, F. C., and Gray, D. L., "Radar Signal Design Subject to Simultaneous Peak and Average Power Constraints," *IEEE Transaction on Information Theory,* Vol. IT-12, Jan. 1966, pp. 13–26.

[3] Heffes, H., and Horing, S., "Optimal Allocation of Tracking Pulses for and Array Radar," *IEEE Transaction on Automatic Control,* Vol. AC-15, No. 1, Feb. 1970, pp. 81–88.

[4] Betts, J. T., "Survey of Numerical Methods for Trajectory Optimization," *Journal of Guidance, Control, and Dynamics*, Vol. 21, No. 2, March–April 1998, pp. 193–207.
doi: 10.2514/2.4231

[5] Enright, P. J., and Conway, B. A., "Discrete Approximations to Optimal Trajectories Using Direct Transcription and Nonlinear Programming," *Journal of Guidance, Control, and Dynamics*, Vol. 15, No. 4, July–Aug. 1992, pp. 994–1002.
doi: 10.2514/3.20934

[6] Fahroo, F., and Ross, I. M., "Costate Estimation by a Legendre Pseudospectral Method," *Journal of Guidance, Control, and Dynamics*, Vol. 24, No. 2, March–April 2001, pp. 270–277.
doi: 10.2514/2.4709

[7] Gelb, A., *Applied Optimal Estimation*, MIT Press, Cambridge, MA, 1984, p. 189.

[8] Athans, M., "The Matrix Minimum Principle," *Information and Control*, Vol. 11, Nov.–Dec. 1996, pp. 592–606.
doi: 10.1016/S0019-9958(67)90803-0

Christoper Rouff
Associate Editor